JOURNAL OF AERONAUTICS AND SPACE TECHNOLOGIES
JANUARY 2007 VOLUME 3 NUMBER 1 (1-9)

NUMERICAL SOLUTION OF 2-D EULER EQUATIONS WITH MULTIGRID

Capt. Murat UYGUN
Turkish Air Force Academy
Dept. of Aeronautical Eng., Yeşilyurt-İSTANBUL
muygun@hho.edu.tr

Kadir KIRKKÖPRÜ
İstanbul Technical University
Dept. of Mechanical Eng., Gümüşsuyu- İSTANBUL
kirkkopruk@itu.edu.tr

ABSTRACT

A multigrid scheme is applied to accelerate the convergence of numerical solution of two dimensional Euler equations to steady state. Cell-centered finite volume method with central differencing scheme is used for discretization. Explicit multistage time-stepping algorithm is used to advance the solution in time. Acceleration techniques including local time stepping and implicit residual smoothing are used as well. Attention is directed towards the accuracy, convergence, and computational performance of the V-cycle and W-cycle multigrid strategies together with piece-wise constant and bilinear interpolations on two grid and three grid levels. Subsonic and transonic inviscid flows past NACA 0012 airfoil are computed as test cases.

Keywords: *Euler Equations, Central Differencing Scheme, Explicit Time-stepping, Multigrid Acceleration.*

1. INTRODUCTION:

In parallel to increase in computational speed, numerical solution of equations governing the fluid flow (Computational Fluid Dynamics) has been regarded as an efficient tool in engineering community. Navier-Stokes equations govern the flows of viscous, heat-conducting fluids [1]. In the limit of vanishing dissipation terms ($\mathrm{Re}\to\infty$), Euler equations governing the flows of inviscid, adiabatic fluids are covered. Due to exclusion of the diffusive effects, the applicability of the Euler equations for flow simulations is limited; the dominating convective character of fluid flows is included though. However, Euler solvers are widely used in a variety of applications for flows past complex geometries.

Time stepping schemes efficiently damp high-frequency error components of the solution but hardly damp low-frequency ones. This degrades the convergence rate considerably. In multigrid method, the convergence is accelerated by damping the low-frequency error components of fine grid solution by means of time stepping on coarser grids. In addition, use of coarse grids allows larger time steps and less computational effort. The early work for the multigrid method is done by Fedorenko [2] and Bakhvalov [3], and later by Brandt [4]. The theory for multigrid is first developed for elliptic problems. However, it is effectively used for hyperbolic problems as well. Brandt surveyed the application of multigrid strategy to computations in fluid dynamics [5]. Ni developed a multigrid scheme for Euler equations [6]. He used cell-vertex formulation and Lax-Wendroff type time-stepping algorithm. Jameson used a multigrid technique in conjunction with cell-centered formulation and multistage time-stepping scheme [7]. Other multigrid techniques were proposed as well [8, 9].

In the current work, a multigrid method based on Full Approximation Storage (FAS) scheme [7, 10, 11] is implemented together with Full Multigrid Algorithm (FMG) [12] to accelerate convergence of numerical solution of two dimensional Euler equations to steady state. A multigrid method on the coarse grid level, which is used to yield a good initial solution for the fine grid level, is called FMG. Cell-centered finite volume discretization technique is adopted. Convective terms are evaluated using central differencing scheme [13]. The flux vectors at the midpoint of a cell face are computed by arithmetic averaging of flow variables at two neighboring cells. Euler equations are integrated in time with multistage explicit Runge-Kutta scheme. The flow solution is advanced at the local maximum speed by using local time stepping [14]. Larger time steps are allowed due to implicit residual smoothing [15-17]. Figure 1 presents the schematic of the full multigrid for four grids. This procedure is known as V (saw-tooth) cycle. The procedure with more cycles on the coarse grids is termed W-cycle (figure 2).

Both V- and W-cycle procedures are used to execute the multigrid strategy. One Runge-Kutta time step before the restriction and no Runge-Kutta time step

after prolongation are done. Residuals and flow variables are restricted from fine to coarse grid by a weighted average. A forcing function is introduced into the time-stepping scheme. Solution corrections are prolongated from coarse to fine grid by piece-wise constant and bilinear interpolations.

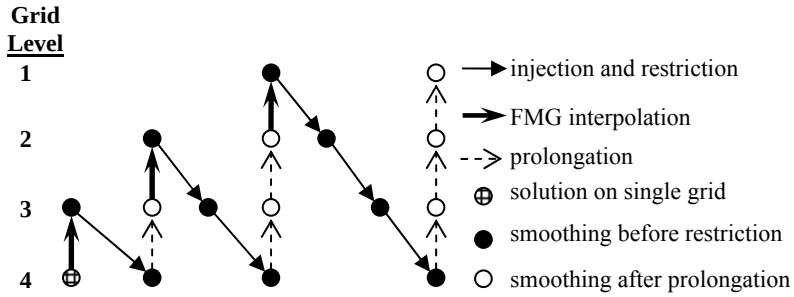

Figure 1. Schematic of the Full Multigrid for four grid levels – V cycle [18]

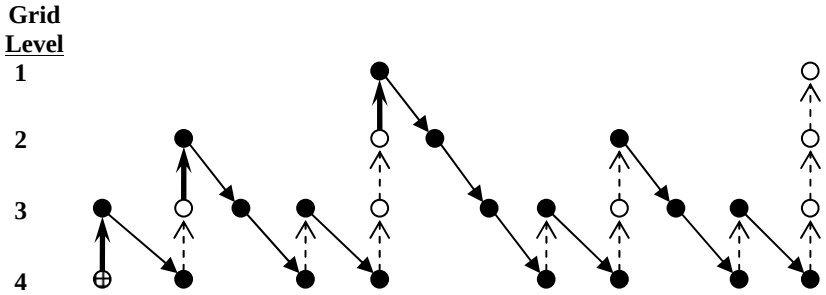

Figure 2. Schematic of the Full Multigrid for four grid levels – W cycle [18]

Implicit smoothing of solution corrections with constant coefficients is used in order to damp the high frequency errors, which are introduced by interpolation of the solution corrections. In case of computations on three grid levels, the FMG method is applied to provide an initial solution for the fine grid. The artificial dissipation model with constant coefficient, second-order differences is used on the coarse grids to reduce computational effort. The same Courant-Friedrichs-Lewy (CFL) number is used on all grids so that larger time steps are used on coarser grids.

Details regarding the formulation, methodology and validation are presented. Subsonic (M=0.63, α=2 deg.) and transonic (M=0.8, α=1.25 deg.) inviscid flows past NACA 0012 are computed as test cases to indicate the effectiveness of the multigrid technique. Computed results are compared to numerical results [19, 20].

2. GOVERNING EQUATIONS:

Euler equations can be cast into integral form as

$$\iint_{\Omega} \frac{\partial \vec{W}}{\partial t} d\Omega + \oint_{\partial\Omega} \vec{F}\vec{n} dS = 0 , \qquad (1)$$

where Ω denotes for the control volume surrounded by the control surface $\partial\Omega$. $\vec{W}$ is the vector of conservative variables, $\vec{F}$ is the convective flux vector. $\vec{n} = n_x\vec{i} + n_y\vec{j}$ is the outer normal vector. $\vec{W}$ and $\vec{F}$ are defined as

$$\vec{W} = \begin{bmatrix} \rho \\ \rho u \\ \rho v \\ \rho E \end{bmatrix} \qquad \vec{F} = \begin{bmatrix} \rho\vec{V} \\ \rho u\vec{V} + p\vec{i} \\ \rho v\vec{V} + p\vec{j} \\ \rho H\vec{V} \end{bmatrix} \qquad (2)$$

The variables $x - y$, t, p, ρ, T, $u - v$ are cartesian coordinates, time, pressure, density, temperature and velocity components respectively. $\vec{i} - \vec{j}$ are unit vectors associated with the cartesian coordinates. E and H denote total energy and total enthalpy. $\vec{V} = u\vec{i} + v\vec{j}$ is the velocity vector. Assuming air as an ideal gas, the equation of state is used to calculate the pressure and temperature;

$$p = (\gamma - 1)\rho\left[E - \frac{u^2 + v^2}{2}\right], \quad T = \frac{p}{\rho R} . \qquad (3)$$

γ is the ratio of specific heats and R is the gas constant.

3. SPATIAL DISCRETIZATION:

Integral form of the Euler equations is solved using cell-centered finite volume method. Computational domain is divided into quadrilateral control volumes (cells). In the cell-centered scheme, flow quantities are associated with the center of a control volume. Finite volume method requires an evaluation of the convective fluxes, which are assumed to be constant along the individual cell face. In this work, convective fluxes are evaluated by means of central differencing scheme [13].

Inviscid flows lack viscous effects. Then, physical diffusion is not adequate to prevent odd-even decoupling of the cell-centered schemes. In order to avoid odd-even decoupling of the solution and oscillations near shocks, stagnation points and boundary layer edges, finite volume scheme requires the addition of artificial dissipation term $\vec{D}$. Then, eq. (1) is written as

$$\iint_{\Omega} \frac{\partial \vec{W}}{\partial t} d\Omega + \oint_{\partial\Omega} \left[\vec{F}\vec{n} dS - \vec{D} \right] = 0 , \quad (4)$$

After writing eq. (4) for all cells and employing method of lines, where spatial and temporal terms are discretized separately, a system of first order ODE is obtained [13]. Approximating the integrals with the mean value theorem, eq. (4) for a particular non-moving cell becomes

$$\Omega_{I,J} \frac{d\vec{W}_{I,J}}{dt} = -\vec{R}\left(\vec{W}_{I,J}\right), \quad (5)$$

where $\vec{R}\left(\vec{W}_{I,J}\right)$ is called the "residual" and is defined as

$$\vec{R}\left(\vec{W}_{I,J}\right) = \sum_{ncf=1}^{4} \left[\vec{F}\vec{n}\Delta S - \vec{D}_{I,J} \right]_{ncf} \quad (6)$$

I and J locate the particular cell and ncf identifies cell faces. ΔS denotes the area of the cell face. Dissipation vector $\vec{D}_{I,J}$, which is a blend of adaptive second and fourth order differences, is defined as [13]

$$\begin{aligned} \vec{D}_{I,J}\left(\vec{W}\right) &= \vec{D}^{I}_{I,J}\left(\vec{W}\right) + \vec{D}^{J}_{I,J}\left(\vec{W}\right) \\ &= \left(\vec{d}_{I+1/2,J} - \vec{d}_{I-1/2,J}\right) + \left(\vec{d}_{I,J+1/2} - \vec{d}_{I,J-1/2}\right) \end{aligned} . \quad (7)$$

Dissipation flux at the cell face is defined as

$$\vec{d}_{I+1/2,J} = \alpha_{I+1/2,J} \left[\varepsilon^{(2)}_{I+1/2,J} \delta^{(1)}_{I} \vec{W}_{I,J} - \varepsilon^{(4)}_{I+1/2,J} \delta^{(3)}_{I} \vec{W}_{I,J} \right], \quad (8)$$

where $\delta^{(1)}$ and $\delta^{(3)}$ are 1st and 3rd order difference operators, which are defined as

$$\begin{aligned} \delta^{(1)}_{I} \vec{W}_{I,J} &= \vec{W}_{I+1,J} - \vec{W}_{I,J} \\ \delta^{(3)}_{I} \vec{W}_{I,J} &= \vec{W}_{I+2,J} - 3\vec{W}_{I+1,J} + 3\vec{W}_{I,J} - \vec{W}_{I-1,J} \end{aligned} . \quad (9)$$

α is a scaling factor, which is written for I direction as [21]

$$\alpha_{I+1/2,J} = \left[\left(\Lambda^{I}_{c}\right)_{I,J} + \left(\Lambda^{I}_{c}\right)_{I+1,J} \right] \Big/ 2 , \quad (10)$$

where

$$\Lambda^{I}_{C} = \left(\left| \vec{V}\vec{n} \right| + c \right) \Delta S^{I} . \quad (11)$$

Λ_C is the spectral radii of the convective flux Jacobian. c is the local speed of sound. The coefficients are computed as

$$\begin{aligned} \varepsilon^{(2)}_{I+1/2,J} &= \kappa^{(2)} \max\left(\nu_{I,J}, \nu_{I+1,J}\right) \\ \varepsilon^{(4)}_{I+1/2,J} &= \max\left[0, \left(\kappa^{(4)} - \varepsilon^{(2)}_{I+1/2,J}\right)\right] \end{aligned} \quad (12)$$

with the pressure sensor given as

$$\nu_{I,J} = \left| \frac{\overline{p}_{I-1,J} - 2\,\overline{p}_{I,J} + \overline{p}_{I+1,J}}{\overline{p}_{I-1,J} + 2\,\overline{p}_{I,J} + \overline{p}_{I+1,J}} \right| . \quad (13)$$

Pressure sensor activates the second-difference dissipation in regions of large pressure gradients and switches it off in smooth regions of flow. $\kappa^{(2)} \approx 1/2$ and $\kappa^{(4)} \approx 1/96$ are typical constants as dissipation coefficients. Dissipation flux is of first order in regions of large pressure gradients and is of third order in smooth regions of flow.

4. TIME INTEGRATION:

After employing explicit Euler scheme, eq. (5) becomes

$$\frac{\vec{W}^{n+1}_{I,J} - \vec{W}^{n}_{I,J}}{\Delta t} = -\frac{1}{\Omega_{I,J}} \vec{R}\left(\vec{W}^{n}_{I,J}\right) \quad (14)$$

Time stepping in eq. (14) is done using M-stage Runge-Kutta scheme, which is defined as

$$\begin{aligned} &\vec{W}^{(0)}_{I,J} = \vec{W}^{(n)}_{I,J} \\ &\vdots \\ &\vec{W}^{(m)}_{I,J} = \vec{W}^{(0)}_{I,J} - \alpha_m \frac{\Delta t_{I,J}}{\Omega_{I,J}} \vec{R}\left(\vec{W}^{(m-1)}_{I,J}\right) \\ &\vdots \\ &\vec{W}^{(n+1)}_{I,J} = \vec{W}^{(M)}_{I,J} \end{aligned} \quad (15)$$

where $m = 1, 2, ..., M$ and $\vec{R}\left(\vec{W}^{(m-1)}_{I,J}\right)$ contains the discretization of the convective and dissipation fluxes in (m-1)th stage. Table 1 presents optimized Runge-Kutta coefficients for maximum stability of a centrally discretized scheme.

Table 1. Optimized Stage Coefficients.

Central Differencing Scheme					
m	1	2	3	4	5
α	1/4	1/6	3/8	1/2	1

Convergence rate of the explicit time-stepping scheme is accelerated using local time stepping, implicit residual smoothing and multigrid.

Local Time Stepping:

The use of local time steps allows the signals propagate at speeds in proportion to cell sizes. Local time step $\Delta t_{I,J}$ for a particular control volume is computed accounting for convective contributions such that [14]

$$\left(\Delta t_C\right)_{I,J} = CFL \frac{\Omega_{I,J}}{\left(\Lambda^{I}_{C} + \Lambda^{J}_{C}\right)_{I,J}} \quad (16)$$

Subscripts I and J locate particular control volume. Superscripts I and J denote the coordinate directions. Λ^{I}_{C} is the spectral radii of the convective flux Jacobian matrix:

$$\Lambda^{I}_{C} = \left| \vec{V}\vec{n} \right| + c\Delta S^{I} , \quad (17)$$

c is the speed of sound. The normal vectors and face areas are obtained by averaging the values at two opposite sides of the control volume in associated coordinate direction.

Implicit Residual Smoothing:

This technique was first introduced by Lerat [22] and later implemented on the Runge-Kutta Stepping scheme by Jameson et.al. [15] in order to extend the stability limit of the scheme. CFL number is increased by replacing the residual at each cell by a weighted average of residuals at neighboring cells. This is done at each stage of the Runge-Kutta Stepping scheme before the solution is updated. In two-dimensional case, residual is smoothed as products of the respective one-dimensional smoothing [16]:

$$\begin{aligned} -\varepsilon^I \tilde{R}_{I-1,J} + \left(1+2\varepsilon^I\right)\tilde{R}_{I,J} - \varepsilon^I \tilde{R}_{I+1,J} &= \vec{R}_{I,J} \\ -\varepsilon^J \hat{R}_{I,J-1} + \left(1+2\varepsilon^J\right)\hat{R}_{I,J} - \varepsilon^J \hat{R}_{I,J+1} &= \tilde{R}_{I,J} \end{aligned}, \qquad (18)$$

where $\tilde{R}_{I,J}$ and $\hat{R}_{I,J}$ denote the smoothed residuals in I and J directions. $\vec{R}_{I,J}$ is the unsmoothed residual. The average is calculated solving the implicit system in eq. (18). The variable smoothing coefficients are defined in two-dimensional case as [17]

$$\varepsilon^I = \max\left\{\frac{1}{4}\left[\left(\frac{CFL^*}{CFL}\frac{\Lambda_C^I}{\Lambda_C^I+\theta\Lambda_C^J}\right)^2 - 1\right], 0\right\}. \qquad (19)$$

$$\varepsilon^J = \max\left\{\frac{1}{4}\left[\left(\frac{CFL^*}{CFL}\frac{\Lambda_C^J}{\theta\Lambda_C^I+\Lambda_C^J}\right)^2 - 1\right], 0\right\}$$

θ is taken as 0.125. CFL^* and CFL are Courant-Friedrichs-Lewy numbers of the smoothed and unsmoothed schemes such that

$$\frac{CFL^*}{CFL} \le \sqrt{1+4\xi} \qquad (20)$$

When $\xi = 0.8$ is used, the value of the ratio becomes about 2 and it means that CFL number can be raised by a factor of 2.

Multigrid Acceleration:

FAS scheme for two grid levels with multigrid V-cycle is described as follows. Eq. (5) on a fine grid, which is denoted by the subscript h, is written as

$$\frac{d\vec{W}_h}{dt} = -\frac{1}{\Omega_h}\vec{R}_h \qquad (21)$$

Coarse grid is obtained by deleting every 2nd line in each coordinate directions and it is denoted by the subscript 2h. With explicit Euler scheme, eq. (21) becomes

$$\frac{\vec{W}_h^{n+1} - \vec{W}_h^n}{\Delta t} = -\frac{1}{\Omega_h}\vec{R}_h\left(\vec{W}_h^n\right). \qquad (22)$$

Calculate the solution on fine grid:

After one time step using explicit multistage scheme, the solution is updated as

$$\left(\vec{W}_h^{n+1}\right)_{I,J} = \left(\vec{W}_h^m\right)_{I,J}, \qquad (23)$$

where $(m=5)$ is the last stage in Runge-Kutta scheme. A new residual $\vec{R}_h\left(\vec{W}_h^{n+1}\right)$ is evaluated with this solution.

Restrict flow variables from fine to the coarse grid:

The solution on the fine grid (h) is injected into the coarse grid (2h) by using a volume weighted average as

$$\vec{W}_{2h}^{(0)} = \sum_{ncv=1}^{4}\left(\Omega_h \vec{W}_h^{n+1}\right)_{ncv} \Big/ \sum_{ncv=1}^{4}\left(\Omega_h\right)_{ncv}, \qquad (24)$$

where the summation is over the four fine grid (h) cells, which build one coarse grid (2h) cell. A new residual $\vec{R}_{2h}\left(\vec{W}_{2h}^{(0)}\right)$ is evaluated with the injected solution.

Restrict residuals from fine to the coarse grid:

In order to smooth the low-frequency error components, the fine grid (h) residuals are restricted to coarse grid (2h) by using a conservative (full-weighting) transfer operator:

$$I_h^{2h}\vec{R}_h\left(\vec{W}_h^{n+1}\right) = \sum_{ncv=1}^{4}\left[\vec{R}_h\left(\vec{W}_h^{n+1}\right)\right]_{ncv}, \qquad (25)$$

where the summation is over the four fine grid cells, which build one coarse grid cell.

Calculate solution on the coarse grid:

After one time step using multistage Runge-Kutta time stepping scheme, the solution on the coarse grid (2h) is calculated as

$$\begin{aligned} &\vec{W}_{2h}^{(0)} = \vec{W}_{2h}^{(n)} \\ &\vdots \\ &\vec{W}_{2h}^{(m)} = \vec{W}_{2h}^{(0)} - \alpha_m \frac{\Delta t_{2h}}{\Omega_{2h}}\mathcal{L}_{IRS}\left(\overrightarrow{RHS}\right)_{2h} \qquad (26) \\ &\vdots \\ &\vec{W}_{2h}^{(n+1)} = \vec{W}_{2h}^{(M)} \end{aligned}$$

where $m = 1, 2, ..., M$ and

$$\left(\overrightarrow{RHS}\right)_{2h} = \vec{R}_{2h}\left(\vec{W}_{2h}^{(m-1)}\right) + \vec{f}_{2h}. \qquad (27)$$

$\mathcal{L}_{IRS}$ denotes implicit residual smoothing operator. In order to keep the solution accuracy of the fine grid on the coarse grid (2h), a forcing function $\vec{f}_{2h}$ is calculated in the first stage of R-K scheme and is frozen for a specified grid level throughout a multigrid cycle. Forcing function is defined as the difference between the residual that is restricted to coarse grid (2h) and the coarse grid residual evaluated using the solution $\vec{W}_{2h}^{(0)}$ that is injected to coarse grid.

$$\vec{f}_{2h} = I_h^{2h}\vec{R}_h\left(\vec{W}_h^{n+1}\right) - \vec{R}_{2h}\left(\vec{W}_{2h}^{(0)}\right). \qquad (28)$$

Using the restriction operator defined in eq. (25), forcing function reads

$$\vec{f}_{2h} = \sum_{ncv=1}^{4} \left[\vec{R}_h \left(\vec{W}_h^{n+1} \right) \right]_{ncv} - \vec{R}_{2h} \left(\vec{W}_{2h}^{(0)} \right). \quad (29)$$

On the following coarse grid (4h) for three grid levels, the residuals on grid levels 2h and 4h together with forcing function on grid level 2h form the forcing function as follows

$$\vec{f}_{4h} = I_{2h}^{4h} \left(\overrightarrow{RHS} \right)_{2h} - \vec{R}_{4h} \left(\vec{W}_{4h}^{(0)} \right), \quad (30)$$

$$\vec{f}_{4h} = \sum_{ncv=1}^{4} \left[\vec{R}_{2h} \left(\vec{W}_{2h}^{n+1} \right) + \vec{f}_{2h} \right]_{ncv} - \vec{R}_{4h} \left(\vec{W}_{4h}^{(0)} \right). \quad (31)$$

This process is repeated until the coarsest grid is reached.

Calculate solution correction on the coarse grid:

After one or several iterations, the solution on the coarse grid is updated. Then, the solution correction at the coarse grid (2h) cell is calculated as

$$\Delta \vec{W}_{2h} = \vec{W}_{2h}^{n+1} - \vec{W}_{2h}^{(0)}, \quad (32)$$

where $\vec{W}_{2h}^{(0)}$ is the solution restricted to coarse grid (2h) before any iterations are performed (eq. 24) and $\vec{W}_{2h}^{n+1}$ is the solution calculated on the coarse grid (eq. 26). Solution corrections are smoothed by using constant coefficient implicit smoothing in order to damp the high frequency errors, which are introduced by interpolation of the solution corrections. Optimum smoothing coefficient can be determined through numerical experiment.

Update solution on the fine grid:

In order to update the solution on the fine grid (h), solution corrections are prolongated to there as follows

$$\left(\vec{W}_h^{n+1} \right)_{I,J} = \left(\vec{W}_h^{(m)} \right)_{I,J} + \left(I_{2h}^{h} \Delta \vec{W}_{2h} \right)_{I,J}, \quad (33)$$

where $\vec{W}_h^{(m)}$ is the solution before the restriction to coarse grid (2h) and is calculated using eq. (23). I_{2h}^{h} is an interpolation operator.

The simplest definition of the prolongation operator is piece-wise constant interpolation, which is defined for 2-D case (figure 3) as

$$\left(I_{2h}^{h} \Delta \vec{W}_{2h} \right)_{I,J} = \left(\Delta \vec{W}_{2h} \right)_{I,J}. \quad (34)$$

Another definition of prolongation operator is bilinear interpolation, which is defined for 2-D case (figure 4) as

$$\left(I_{2h}^{h} \Delta \vec{W}_{2h} \right)_{I,J} = \frac{1}{16} \left[9 \left(\Delta \vec{W}_{2h} \right)_{I,J} + 3 \left(\Delta \vec{W}_{2h} \right)_{I+1,J} + 3 \left(\Delta \vec{W}_{2h} \right)_{I,J+1} + \left(\Delta \vec{W}_{2h} \right)_{I+1,J+1} \right]. \quad (35)$$

Accuracy of Transfer Operators

Orders of prolongation and restriction operators depend on the order of governing system of equations to be solved. In order to damp low frequency errors, it should be satisfied that [18, 23]

$$m_{\text{Res}} + m_{\text{Pro}} > m_{\text{Eqn}} \quad (36)$$

where m_{Res} and m_{Pro} denote the order of restriction and prolongation operators. The order of piece-wise constant interpolation (eq. 34) is zero. Both bilinear interpolation (eq. 35) and full-weighting restriction (eq. 24) have orders of two. m_{Eqn} denotes the order of governing equations and $m_{\text{Eqn}} = 1$ for Euler equations and $m_{\text{Eqn}} = 2$ for Navier-Stokes equations. If Euler equations are solved, prolongation operator with piece-wise constant interpolation satisfies the condition. In case of viscous flows, prolongation operator with bilinear interpolation is required to satisfy the condition.

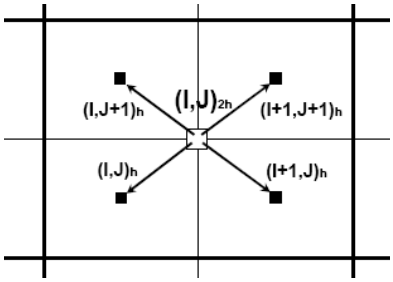

Figure 3. Schematic for the piece-wise constant prolongation

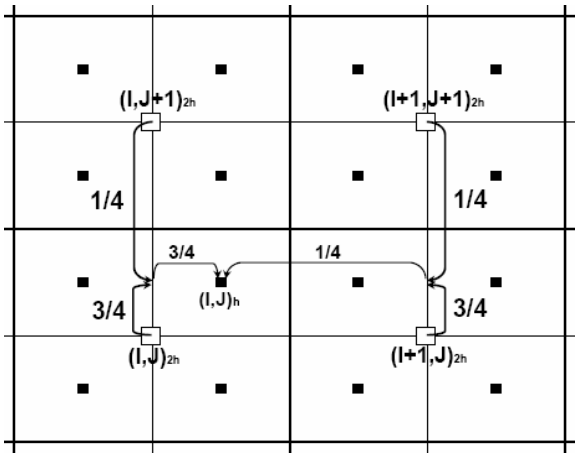

Figure 4. Schematic for the bilinear prolongation

5. BOUNDARY CONDITIONS:

Boundary conditions on all grid levels are treated in the same way. Two layers of ghost cells are utilized. At the solid wall, flow tangency is maintained and the normal derivative of temperature is zero (adiabatic wall). The wall pressure is obtained by extrapolation from the interior domain. A continuity condition is enforced along the wake cut in the C-type grid. Characteristic boundary condition is applied to the farfield boundaries. Boundary conditions are frozen on the coarse grids and updated on the fine grid only after each smoothing step.

6. COMPUTATIONAL RESULTS:

The numerical results given here demonstrate the accuracy and computational efficiency of the multigrid method for inviscid flows. For all computations, C-type computational grid including 224x48 cells with 128 cells on the airfoil, and 48 cells in the wake is used (figure 5). The outer boundary is located 15 chords away from the airfoil. The grid spacing next to the wall is $5x10^{-3}$ chord lengths. Both V- and W-cycle procedures with piece-wise constant and bilinear interpolations on two grid levels and three grid levels with FMG are used to execute the multigrid strategy. One Runge-Kutta time step before the restriction and no Runge-Kutta time step after prolongation are done. Residuals and flow variables are restricted from fine to coarse grid by a weighted average. A forcing function is introduced into the time-stepping scheme. Solution corrections are prolongated from coarse to fine grid by piece-wise constant and bilinear interpolations. Implicit smoothing of solution corrections with constant coefficients is used in order to damp the high frequency errors, which are introduced by interpolation of the solution corrections. In case of computations on three grid levels, the FMG method is applied to provide an initial solution for the fine grid. The artificial dissipation model with constant coefficient, second-order differences is used on the coarse grids to reduce computational effort. The CFL number of 7.5 is used on all grids so that larger time steps are used on coarser grids. Convergence is monitored using L_2 norm of density residual. All computations were performed on a PC including 512 Mb memory and two GHz CPU running Windows XP.

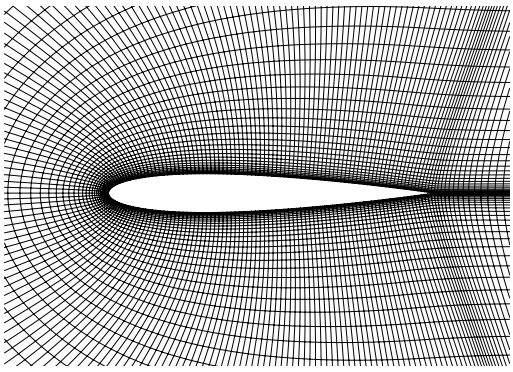

Figure 5. Computational grid around NACA 0012

First test case involves subsonic flow past NACA 0012 airfoil at free stream Mach number of 0.63 and incidence angle of 2 degrees [19]. Figure 6a compares the convergence rates between a single grid level, two grid levels and three grid levels with FMG computations. Multigrid computations are performed using V-cycle procedure and piece-wise constant interpolation.

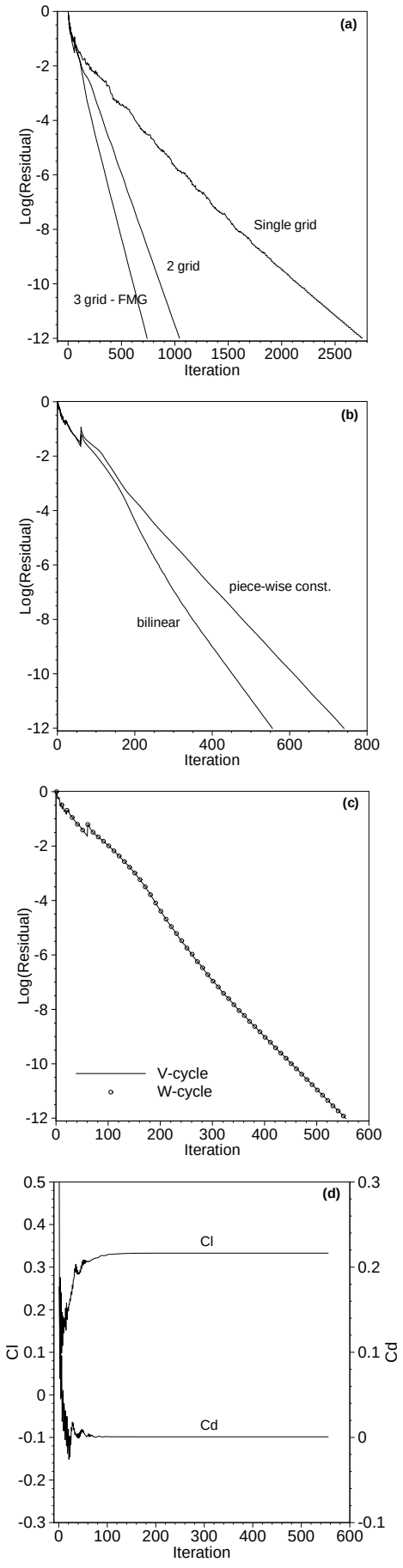

Figure 6. Computed results

Convergence rate is increased by a factor of about 2.6 on using the two grid levels and by a factor of about 3.7 on using the three grid levels with FMG. Figure 6b compares the convergence rates between piece-wise constant and bilinear interpolations on three grid levels with FMG. Convergence rate is further increased by a factor of 1.3 due to bilinear interpolation. Figure 6c compares the convergence rates between V-cycle and W-cycle procedures with bilinear interpolation on three grid levels with FMG. There is no noticeable difference between computed convergence rates. Figure 6d indicates the lift and drag histories computed using V-cycle procedure and bilinear interpolation on three grid levels with FMG.

Figure 7 and 8 indicate the pressure distribution and pressure losses on the airfoil surface, respectively. The results for a single grid level and three grid levels are compared. There is no noticeable difference between computed results.

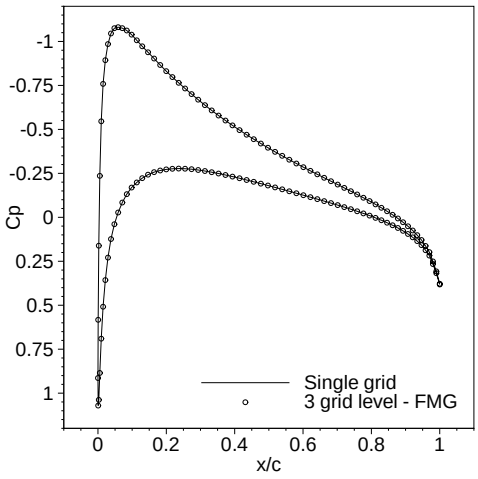

Figure 7. Pressure distribution

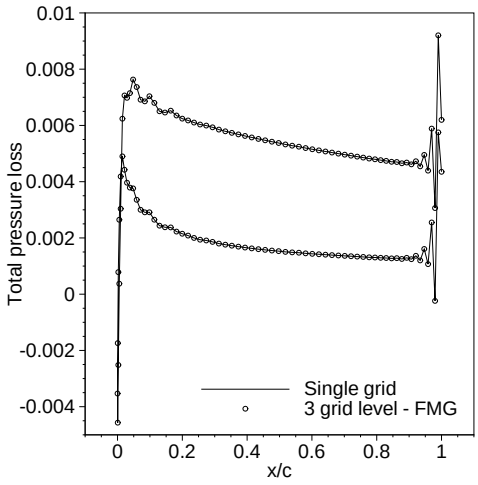

Figure 8. Total pressure losses

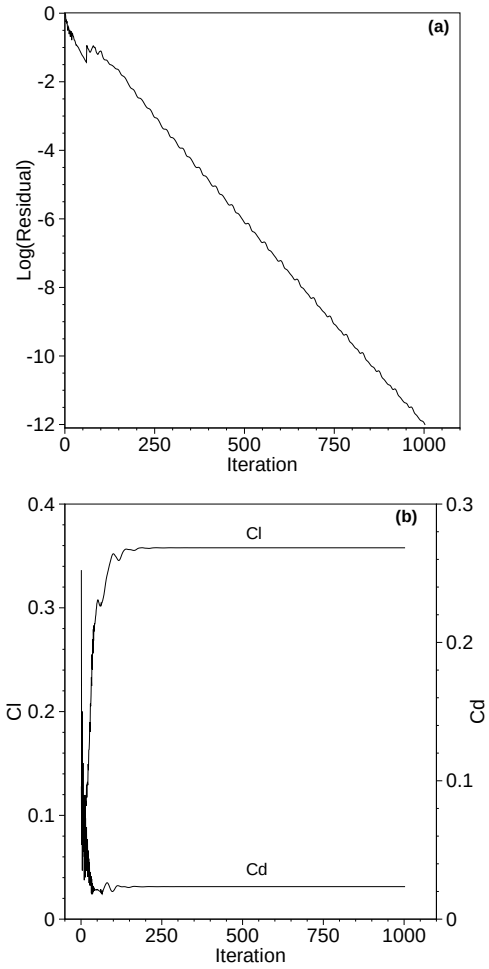

Figure 9. Convergence and lift-drag histories

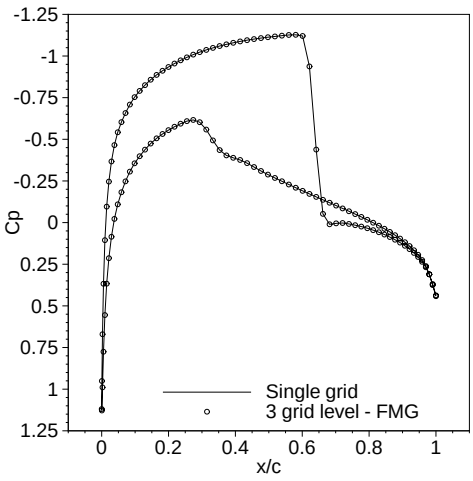

Figure 10. Pressure distribution

Second test case involves transonic flow past a NACA 0012 airfoil at free stream Mach number of 0.8 and incidence angle of 1.25 degrees [20]. The convergence and lift-drag histories are shown in figure 9. Computed results are obtained using V-cycle procedure and bilinear interpolation on three grid levels with FMG. The pressure distribution and total pressure losses are shown in figure 10 and figure 11.

Results computed on single grid and three grid levels agree with each other as well as with those presented in ref. [20]. Iso-Mach contours with ΔM=0.05 are shown in figure 12. Computed iso-Mach contours are similar to those presented in reference [20].

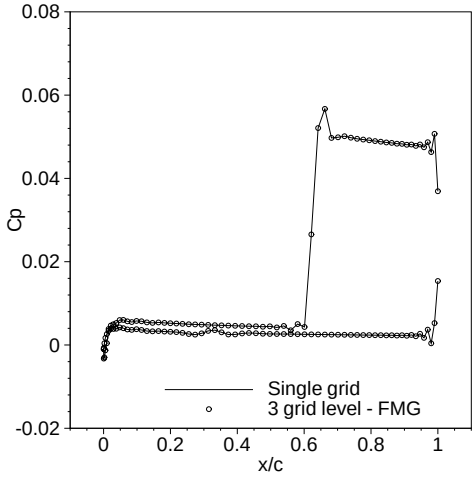

Figure 11. Total pressure losses

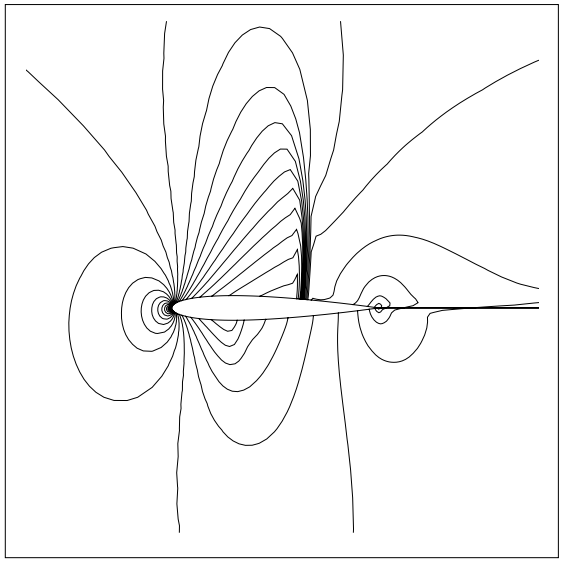

Figure 12. Iso-Mach contours with ΔM=0.05

7. CONCLUSIONS:

A multigrid scheme is implemented into an existing two dimensional Euler solver in order to accelerate convergence to steady state. Subsonic and transonic inviscid flows past NACA 0012 airfoil are computed as test cases. Convergence down to machine zero is attained in the computations. Computed results agree well with those available in the literature and they indicate that multigrid scheme is successfully applied. When the multigrid scheme with bilinear interpolation on three grid level with FMG is used, convergence rate is increased by a factor of about 5. No significant difference between convergence rates of V-cycle and W-cycle computations is observed.

In the case of bilinear prolongation on non-uniform grids, it will be better grid-weighted averages are taken into account due to uneven distances between cell centers.

8. REFERENCES:

[1] Wilcox, D.C.; "Turbulence Modeling for CFD," DCW Industries Inc., La Canada, California, USA, 1993.

[2] Fedorenko, R.P.; "A Relaxation Method for Solving Elliptic Difference Equations," USSR Comput. Math. and Phys. Vol. 1, pp.1092-1096, 1961.

[3] Bakhvalov, N.S.; "On the Convergence of A Relaxation Method with Natural Constraints on the Elliptic Operator," USSR Comput. Math. and Phys. Vol. 6, pp.101-135, 1966.

[4] Brandt, A., "A Multilevel Adaptive Solutions of Boundary Value Problems," Mathematics of Computation Vol. 31, pp. 333-390, 1977.

[5] Brandt, A.; "Multi-level Adaptive Computations in Fluid Dynamics," AIAA 79-1455, 1979.

[6] Ni, R.H.; "A multiple Grid Scheme for solving the Euler Equations," AIAA Journal, Vol.20, pp.1565-1571, Nov. 1982.

[7] Jameson, A.; "Solution of the Euler Equations fro Two-dimensional, Transonic Flow by a Multigrid Method," Applied Mathematics and Computation, Vol. 13, pp.327-356, 1983.

[8] Hall, M.G.; "Cell vertex multigrid schemes for solution of the Euler equations," In Proc. IMA Conference on Numerical Methods for Fluid Dynamics, Reading, April 1985.

[9] Hemker, P.W., Spekreijse, S.P.; "Multigrid Solution of the Steady Euler Equations," Advances in multigrid methods, series: Notes Numer. Fluid Mech. Vol. 11, pp. 33-44, Oberwolfach, 1984.

[10] Jameson, A.; "Multigrid Algorithms for Compressible Flow Calculations," Mechanical and Aerospace Engineering Report 1743, Princeton Univ. NJ, Proceedings of the Second European Conference on Multigrid Methods, Cologne, October 1985.

[11] Martinelli, L., Jameson, A. and Grasso, F.; "A Multigrid Method for the Navier-Stokes Equations," AIAA 86-0208, Jan. 1986.

[12] Brandt, A.; "Guide to Multigrid Development, Multigrid Methods I," Lecture Notes in Mathematics, No.960, Springer Verlag, New York, 1981.

[13] Jameson, A., Schmidt, W., Turkel, E.; "Numerical Solutions of the Euler Equations by Finite Volume Methods Using Runge-Kutta Time-Stepping Schemes," AIAA Paper 81-1259, AIAA 14th Fluid and Plasma Dynamic Conference, June 1981.

[14] Arnone, A.; Liou, M.S.; Povinelli, L.A.; "Integration of Navier-Stokes Equations Using Dual Time Stepping and a Multigrid Method," AIAA Journal, Vol.33, No. 6, pp. 985-990, June 1995.

[15] Jameson, A., Baker, T. J. "Solution of the Euler Equation for Complex Configurations," AIAA Paper 83-1929, Proceedings of 6th AIAA Computational Fluid Dynamics Conference, Danvers, July 1983.

[16] Jameson, A., "Transonic Flow Calculations," Princeton University Report MAE 1651, March 1984, in Numerical Methods in Fluid Dynamics, edited by F. Brezzi, Lecture Notes in Mathematics, Vol. 1127, Springer-Verlag, pp. 156-242, 1985.

[17] Martinelli, L., Jameson, A.; "Validation of a Multigrid Method for the Reynolds Averaged Equations," AIAA 88-0414, 1988.

[18] Trottenberg, U. Oosterlee, C., Schüller, A.; "Multigrid," Academic Press, London, UK, 2001.

[19] Lock, R.C.; "Test Cases for Numerical Methods in Two Dimensional Transonic Flows," Report AGARD-R-575-70, North Atlantic Treaty Organization Advisory Group for Aerospace Research and Development, 1970.

[20] North Atlantic Treaty Organization, "Test Cases for Inviscid Flow Field Methods," Advisory Report AGARD-AR-211, North Atlantic Treaty Organization Advisory Group for Aerospace Research and Development, 1985, Report of Fluid Dynamics Panel Working Group 07.

[21] Blazek, J.; "Verfahren zur Beschleunigung der Lösung der Euler- und Navier–Stokes Gleichungen bei stationaren Über-und Hyperschallströmungen," Ph.D. Thesis, University of Braunschweig, 1994.

[22] Lerat, A., "Une Classe de Schemas aux Differences Implicites Pour les Systemes Hyperboliques de Lois de conservation," Comptes Rendus Acad. Sciences Paris, Vol.288A.

[23] Hemker, P.W.; "On the Order of Prolongations and Restrictions in Multigrid Procedures," Journal of Computational and Applied Mathematics, Vol. 32, pp. 423-429, 1990.

VITA

Capt. Murat UYGUN

He was graduated from Aeronautical Engineering Department at Turkish Air Force Academy, Istanbul in August 1995. He received his M.Sc. degree in Aerospace Engineering from Middle East Technical University, Ankara in September 2000. Later, he joined Aeronautical Engineering Department at Turkish Air Force Academy, Istanbul. His thesis and follow-on work as a PhD student in Mechanical Engineering at Istanbul Technical University, involves numerical simulation of internal and external viscous flow fields. During 2002-2003, he conducted a study as a NATO Fellow at Defence Research Development Canada-Atlantic (DRDC-Atlantic), Halifax, Canada. His current research interests are Computational Fluid Dynamics, Finite Volume Method, low Mach number preconditioning, convergence acceleration techniques, deforming grids and turbulence modeling.

Kadir KIRKKÖPRÜ

He obtained his BS and M.Sc. degrees from Mechanical Engineering Department at Istanbul Technical University (ITU) in 1979 and 1981, respectively. He received his PhD degree in Mechanical Engineering from the University of Colorado (CU) at Boulder in 1988. He was Senior Research Associate in Mathematics and Physics Department at the University of East Anglia in England between 1988 and 1990. He joined Mechanical Engineering Department at ITU in 1990. Later, he worked in the Applied Mathematics Department at CU Boulder for two years. He has been professor in Mechanical Engineering Department at ITU since 1998. His main research interests are Analytical and Computational Fluid Dynamics, Fluid Machinery, Asymptotic Techniques and Theoretical Combustion.